Development of Carbon Nanofibers/Pt Nanocomposites for Fuel Cell Application

K. Y. Mudi, A. S. Abdulkareem, A. S. Kovo, O. S. Azeez, J. O. Tijani & E. J. Eterigho

Arabian Journal for Science and Engineering

ISSN 2193-567X
Volume 45
Number 9

Arab J Sci Eng (2020) 45:7329-7346
DOI 10.1007/s13369-020-04498-3

Springer

Arabian Journal for Science and Engineering (2020) 45:7329–7346
https://doi.org/10.1007/s13369-020-04498-3

RESEARCH ARTICLE-CHEMICAL ENGINEERING

Development of Carbon Nanofibers/Pt Nanocomposites for Fuel Cell Application

K. Y. Mudi[1,2,3] · A. S. Abdulkareem[1,2] · A. S. Kovo[1,2] · O. S. Azeez[1] · J. O. Tijani[2,4] · E. J. Eterigho[1]

Received: 3 October 2019 / Accepted: 28 March 2020 / Published online: 22 April 2020

Abstract

Carbon nanofibers (CNFs) were prepared via the deposition of acetylene gas on bimetallic catalyst (Fe–Co) supported on kaolin in a catalytic chemical vapour reactor. Carbon nanofibers/Pt nanocomposite (Pt catalyst) was synthesized by immobilization of potassium tetrachloroplatinate (IV) (K_2PtCl_4) onto the carbon nanofibers (CNFs) by a wet impregnation method. The effects of mass of carbon nanofibers (CNFs) (0.25–0.30 g) and deposition time (150–180 min) on the percentage of platinum (Pt) deposited on the nanofiber were investigated. The developed CNFs/Pt was characterized using different analytical tools such as HRSEM, EDS, HRTEM, BET, TGA, XRD, XPS and cyclic voltammetry (CV). The XRD patterns revealed the crystallite size of the Pt catalyst ranged between 5.54 and 6.69 nm, and the size decreased with increasing mass of support (CNFs). The HRTEM/HRSEM analysis of the CNFs/Pt catalyst showed that the dispersion and distribution pattern and the shape of the catalyst changes as the amount of CNFs increased from 0.25 to 0.3 g. However, deposition time did not influence the crystalline nature of the catalysts. XPS analysis demonstrated the existence of different oxidation states of Pt particles on the surface of CNFs. The CV analysis revealed that CNFs/Pt catalyst supports the oxygen reduction reaction and hydrogen oxidation reaction in the fuel cell. The platinum loading of 0.002–0.004 mg_{pt}/cm^2 in the fabricated electrodes using the developed CNFs/Pt nanocomposite was compared well with other electrodes (fabricated with other support materials) such as carbon black, carbon nanotubes, aerogel and titanium.

Keywords Pt catalyst · Carbon nanofiber · Nanoparticles · Characterization · Wet impregnation · Cyclic voltammetry

1 Introduction

The global search for alternative energy has brought about the use of fuel cell. Fuel Cell (FC), a device for conversion of chemical energy to electrical energy, was considered due to its efficiency, easy to operate and environmental friendliness [1]. There are three basic components of FC, namely the membrane, the electrode and gas diffusion layer called membrane electrode assembly (MEA). The functions of the components include: transport electrons between the electrodes, carry out electrochemical reactions and guide the diffusion layer, respectively [2]. Pt catalysts are employed in FC to aid electrochemical reactions at the electrodes [3]. The choice of Pt in its elemental form is attributed to its ability to resist corrosion, while it remains chemically active to allow adsorption of ions from fuel and oxygen from air on its surface for effective reactions. Also, selectivity as well as its stability that supersedes other metals makes it the right choice for electrode development [4]. Among all factors that affect the electrocatalytic activity of the electrodes in FC, particle size distribution plays a crucial role [5]. The synthesis of Pt in its nano form compared to bulk nature usually enhances particle size and distribution of Pt particles on the support. Not only have that, Pt in nanosize range guaranteed improved surface area and simultaneous occurrence of three phase reactions at the electrode surface.

Despite the advantages of FC in relation to its numerous applications, its disadvantages constitute serious setback to

✉ K. Y. Mudi
m.kehinde@kadunapolytechnic.edu.ng

1 Department of Chemical Engineering, Federal University of Technology, Minna, Niger State, Nigeria

2 Nanotechnology Research Group, Centre for Genetic Engineering and Biotechnology, Federal University of Technology, Minna, Niger State, Nigeria

3 Department of Chemical Engineering, Kaduna Polytechnic, Kaduna, Kaduna State, Nigeria

4 Department of Chemistry, Federal University of Technology, Minna, Niger State, Nigeria

its mass market commercialization. These obstacles include short-time durability and carbon monoxide poisoning due to the Pt used as catalyst in the electrodes [6]. The short-term durability of FC is also caused by Pt agglomeration which restricts its mobility. Carbon monoxide poisoning is due to the introduction of trace amount of carbon monoxide during reforming process of hydrogen production. The itemized shortcomings usually lead to reduction in the FC ability to convert chemical energy to electrical energy, leading to low efficiency. Hence, there is the need for the development of a catalyst electrode with high surface area that will promote the electrochemical reactions. To address this problem, a supported Pt catalyst is employed as electrode materials.

Carbon black has been widely considered as a choice support material in Pt catalyst synthesis. On the other hand, the dense structure and corrosive nature of carbon black when used continually affect the performance of FC [1]. In other to solve these problems associated with the use of carbon black as a supported material for Pt catalyst synthesis, carbon nanofibers (CNFs) of unique structures and better properties, good structural arrangements, chemical stability, mechanical strength and electrical conductivity have been recognized a perfect alternative to carbon black. Additionally, CNFs as an alternative candidate can impact better durability to the electrode and improve the catalyst activity of Pt compared to carbon black.

Many researchers have synthesized Pt catalysts by various methods. For instance, Afolabi [1], Aritonang et al. [3] and David et al. [7] individually reported the preparation of Pt catalyst by impregnation of metallic nanoparticles on a nanomaterial support with the aid of a dispersant. This was followed by oven drying to remove the moisture and finally calcination to remove the residual moisture by reduction and conversion of the salt into their respective oxides. Seth et al. [8] and Wenzhen et al. [9] independently employed polyol method to synthesis Pt nanoparticles in ethylene glycol, followed by modification with sodium hydroxide to control the solution pH for effective particle size reduction. Other methods employed by other researchers include microwave-assisted polyol [10], magnetron sputtering [11], microemulsion [12], supercritical fluid chemical deposition [13] and electrochemical method [14, 15]. However, based on simplicity, impregnation–reduction method has been widely chosen by researchers [1, 3, 7].

The most applied source of Pt nanoparticles is the chloroplatinic acid (H_2PtCl_6) using a dispersant such as the formaldehyde, hydrazine, borohydrates and ethylene glycol [16]. These dispersants also serve as reducing agent and solvent for homogenous dissolution of Pt salt to form solution. The performance of Pt particles depends on the synthesis parameters such as mass of support, precursor concentration [3], temperature and deposition time [1], types of reducing agents used and the precursor types. The Pt particles have been synthesized using precursor such as K_2PtCl_4 by other researchers. For instance, Aritonang et al. [3] synthesized Pt nanoparticles from solution of K_2PtCl_4 using a matrix of bacterial cellulose (BC). The precursor concentrations were varied between 3 and 30 mM. The results of their findings indicated that Pt particle sizes obtained from XRD analysis ranged from 6.3 to 9.3 nm and this particle size increases with increase in the precursor concentration. The effects of deposition technique (conventional refluxing and microwave irradiation), water content, carbon support and metal loading on the average Pt particle size and electrochemically active surface area (ECSA) using polyol deposition process on carbon nanotube (CNT)–CNFs support were reported by Seth et al. [8]. Other researchers who used CNFs as support for synthesis of Pt nanoparticles include: Mineo and Masaru [17] and Sergey et al. [11]. They used supercritical fluid chemical deposition and sputtering deposition methods, respectively, for the deposition of Pt particles on the CNFs. Sergey et al. [18] reported the effect of the surface chemistry of the carbon support on the physicochemical and electrochemical properties of Pt catalyst.

Furthermore, Bassel et al. [19] demonstrated the potentials of graphitic nanofibers-supported platinum catalyst as an electrode for fuel cell application. The authors found that 5 wt% sample exhibited higher performance in comparison with a 25 wt% platinum in Vulcan carbon with low poisoning. Also, the electrochemical activity of the developed electrode was studied, but the performance of the developed electrode was not tested in a fuel cell stack.

Similarly, Antolini [20] reported the formation, microstructural characteristics and stability of carbon-supported platinum catalyst for low-temperature fuel cells. The author opined that preparation method had a great influence in the choice of carbon support and the distribution pattern of the platinum nanoparticles. The amount of platinum in the Pt/C catalyst by impregnation method induced more oxygen sites on the carbon surface and hence high oxidation activity at the electrode in comparison with colloidal method. The authors reviewed a comparison between various preparation methods for carbon-supported platinum catalyst using preparation methods. However, this present work is on the use of carbon nanofibers-supported platinum catalyst as electrode in low-temperature fuel cell. In furtherance of Antolini 2003, Kvande et al. [21] also revealed that low platinum loading is a function of preparation methods.

This reports for the first time the effect of variation of mass of support (CNFs) in relation to the amount of Pt nanoparticles adsorbed for electrochemical reactions. Mass of support, a parameter which has great impact on the size and morphology of the Pt nanoparticles, forms the basis of this study. The prepared CNFs/Pt was characterized using different analytical tools, and the fuel cell application of the materials was evaluated using cyclic voltammetry.

2 Methodology

2.1 Synthesis of Carbon Nanofiber

Carbon nanofibers (CNFs) were synthesized by the decomposition of acetylene (C_2H_2) gas in a CVD reactor. In this case, 0.5 g of the catalyst was stacked into a quartz boat (120 mm × 15 mm) at room temperature and placed at the centre of the tube. The furnace was set at 10 °C/min starting at room temperature, while argon gas was allowed to flow over the catalyst at rate of 472 ml/min. Once the set reaction temperature of 550 °C was attained, the argon flow rate was adjusted and after which carbon source (C_2H_2/H_2 gas mixture) was introduced. The reaction was then allowed to proceed until 40 min reaction time was attained, after which the carbon source flow was stopped and the furnace was allowed to cool down to room temperature under a continuous flow of argon. The boat was then removed from the reactor and re-weighed to quantify the amount of CNF produced. Percentage of CNFs produced was determined using Eq. (1)

$$\%\ \text{CNFs} = \frac{M_{\text{total}} - M_{\text{catalyst}}}{M_{\text{catalyst}}} \times 100 \tag{1}$$

where M_{total} is the total mass of the final catalyst and CNFs produced after CVD reaction process and M_{catalyst} is the initial mess of Fe–Co/kaolin catalyst introduced into the CVD reactor.

2.2 Purification of CNFs

In the purification process, 1 g of as-produced CNFs was weighed and placed inside a 50 ml beaker containing 30 ml of distilled water. 0.1 M HNO_3 and H_2SO_4 mixture (v/v 3:1) was then added to the as-synthesized CNFs in the beaker to remove the impurities present. Distilled water was added to make the content up to 100 ml. The mixture was stirred vigorously and then sonicated for 90 min at 40 °C in an ultrasonic bath to introduce oxygen group to the surface of the treated CNFs so as to open the edges for substrate binding. The oxidized CNFs were then cooled to room temperature, and 300 ml of distilled water was added to wash off the acid and the washing continued until the pH became neutral. The slurry was filtered and the residue oven dried at 120 °C for 12 h. The dried CNFs were grinded and sonicated to prevent agglomeration, and the purified CNFs were then characterized to determine the surface area, functional groups and morphology.

2.3 Synthesis of CNFs/Pt

A known concentration (20 mM) of K_2PtCl_4 stock solution was prepared. Absorbance profiles of this working solution were obtained using ultraviolet visible (UV) spectroscopy to determine the absorbance of different concentrations of the platinic salt at a specific Pt wavelength of 320 nm. Serial dilutions of this solution were prepared and used to plot the calibration curve. This serves as a basis for the determination of the adsorbed Pt on the CNFs support. 0.1 g of purified CNFs was mixed with a 5% polyethylene glycol (PEG) solution and stirred vigorously using magnetic stirrer for 4 h. A known volume of prepared working solution of Pt was then added to the mixture and allowed to be mixed via continuous stirring for about 2 h, after which the slurry was filtered. The absorbance of the filtrate was determined using a UV spectroscopy. The concentration of this solution was then determined using the calibration curve from its initial working solution. The difference between this concentration and the initial concentration gives the concentration of the adsorbed Pt on the CNFs. The CNF/Pt nanocomposite formed as residue was dried in an oven at 120 °C for 12 h and then calcined at 300 °C for 16 h.

2.4 Characterization of CNFs/Pt Catalyst

The CNF/Pt composite was characterized using thermogravimetric analysis (TGA 4000, PerkinElmer, USA) to determine the thermal stability. Brunauer–Emmett–Teller (BET; NOVA 4200e, Quantachrome Instruments, USA) was utilized to determine the surface area based on nitrogen adsorption–desorption isotherm. The degree of crystallinity, morphology, elemental compositions and microstructure of the samples were determined using X-ray diffractometer (XRD; PW 1800 diffractometer, Philips, Netherlands), high-resolution scanning electron microscope coupled with electron diffraction spectrometer (HRSEM-EDX; Zeiss Auriga) and high-resolution transmission electron microscope (HRTEM, Zeiss Auriga). The surface oxidation states of the CNFs were determined using X-ray photoelectron spectroscopy (XPS). Cyclic voltammetry (CV) was used to determine the electrochemical properties of the developed electrode.

2.5 Electrochemical Measurements of CNFs/Pt Catalyst

A slurry of the CNFs/Pt composite was prepared by dissolving a known quantity of platinum-CNF/5% nafion solution in distilled water. The slurry was then sonicated for 3 h, and the cyclic voltammetry (CV) analysis of the slurry was conducted to determine the real electrochemical surface area, rate of reaction, roughness factor and catalyst utilization.

CV procedure entails the use of a conventional air–tight three-electrode cell using 0.5 M H_2SO_4 electrolyte at room temperature. The electrochemical measurements were carried out with a computer controlled potentiostat (663 VA Stand Metrohm) which consists of a platinum wire counter electrode and Ag/AgCl saturated in KCl salt bridge as the reference electrode. The working electrode was a 7-mm-diameter glassy carbon electrode. The cathode of the cell was connected to the working electrode and the anode to the reference and counter electrodes of the potentiostat. The cathode was fed with deionized (DI) water (N_2 was purged to DI water for about 30 min before it was fed to the cathode) at 1.0 ml min^{-1}, and anode was fed with the hydrogen gas at 20.0 ml min^{-1}.

2.6 Performance Evaluation of the MEA in a Fuel Cell Stack

Carbon cloth (Espeed Logistic International Limited, Hong Kong) of 310 μm thickness was cut into 5 by 5 cm taking into consideration that the reaction surface area was 25 cm^2. An ink of the catalyst was formed by mixing 600 mg of 5% nafion solution with 50 mg of CNFs/Pt catalyst powder, and the mixture was sonicated for 30 min. 300 mg isopropanol was then added and stirred. The mixture was then poured into the spraying equipment and fitted with argon at 1.5 MPa pressure. A low-pressure spraying technique was used to spray the catalyst on one side of the carbon cloth. The resulting catalyst electrode sample was allowed to dry at room temperature before it was coupled with a nafion membrane to make the MEA unit. The MEA unit formed from the coated surface of the fabricated electrodes, and the treated membrane was sandwiched and the unit hot pressed at 100 °C and pressure of about 1196 kN/m^2 for 3 min. The resultant unit was cooled to room temperature.

The performance of the fabricated MEAs was tested in a single FC consisting of two graphite plates, the gaskets containing the gas inlet and outlet and ribbed grooved channels for distribution of the fuel gases behind the porous gas–diffusion electrodes. The MEA was placed between the two graphite plates with the Teflon coated gasket placed between the membrane and each of the graphite plates to prevent leakage, and to avoid excessive compression of the electrodes. Copper wires were used as current collectors and were positioned behind the graphite plates. Two stainless steel end plates with bolts and nuts were used to compress the overall assembly, with Teflon sheets for electric insulation placed between the single cell and the end plates.

The single cell was installed in a FC stack equipped with gas sources, temperature control, gas flow–rate control rotameters, back pressure regulators for both hydrogen and oxygen and a load of resistant box. High purity (99.99%) hydrogen and oxygen gases (Afrox, South Africa) were used in the operation as fuel and oxidant, respectively. Hydrogen was passed through a humidifier at room temperature to wet the gas and was fed into the anode at an excess flow rate of 712 ml/min and 20 kPa, while humidified oxygen entered the fuel cell through the cathode at an excess flow rate of 433 ml/min and 15 kPa. The electrons generated from the anode were connected to a digital multimeter (1906 Competing Multimeter), with an external variable resistance to measure the current and voltage produced by the cell. The multimeter was used to measure the voltage and current with an accuracy of ± 0.001 V and ± 0.001 A, respectively. The cell performance of each MEA was determined from its polarization curve, plotted between voltage and current voltage. The power density was also calculated. The results of the performance evaluation of the developed MEA from the Pt–CNF composite are presented in Table 7.

Table 1 BET results of as-received and purified CNF

	As-produced CNF	Purified CNF
BET surface area (m^2/g)	397.8	592.9
Pore volume (cm^3/g)	0.162	0.212
Pore size (nm)	2.88	3.148

2.7 Results and Discussion

This present work investigates the electrochemical and thermal stability of CNFs/Pt nanocomposites. Prior to the formulation, CNFs were synthesized by CVD method followed by purification of as-produced CNFs. The as-produced and purified CNFs were characterized, and the results are hereby presented.

Presented in Table 1 is the BET surface area of as-produced and purified CNFs.

From the result presented in Table 1, the BET surface area, pore volume and pore size of as-produced CNFs were found to be 397.8 m^2/g, 0.162 cm^3/g and 2.88 nm, respectively. The high surface area exhibited by the as-produced CNFs shows that it will be a good electrode material for energy storage facilities. After purification, the surface area, pore volume and pore size increased to 592.9 m^2/g, 0.212 cm^3/g and 3.148 nm, respectively. The increase in surface area of the CNFs after purification might be associated with the creation of more bonds on the surface of the CNFs by the acids used. Also, during this process of acid treatments, residual catalysts were removed as well as impurities thus allowing more spreading of CNFs particles within the fibre structures and hence increase in the amount of surface available as anchoring sites for substrate adsorption. This large surface area could provide the required three phase reaction zones when used as a support, in line with the work of Asanda [22]. The increase in both the pore volume and pore size

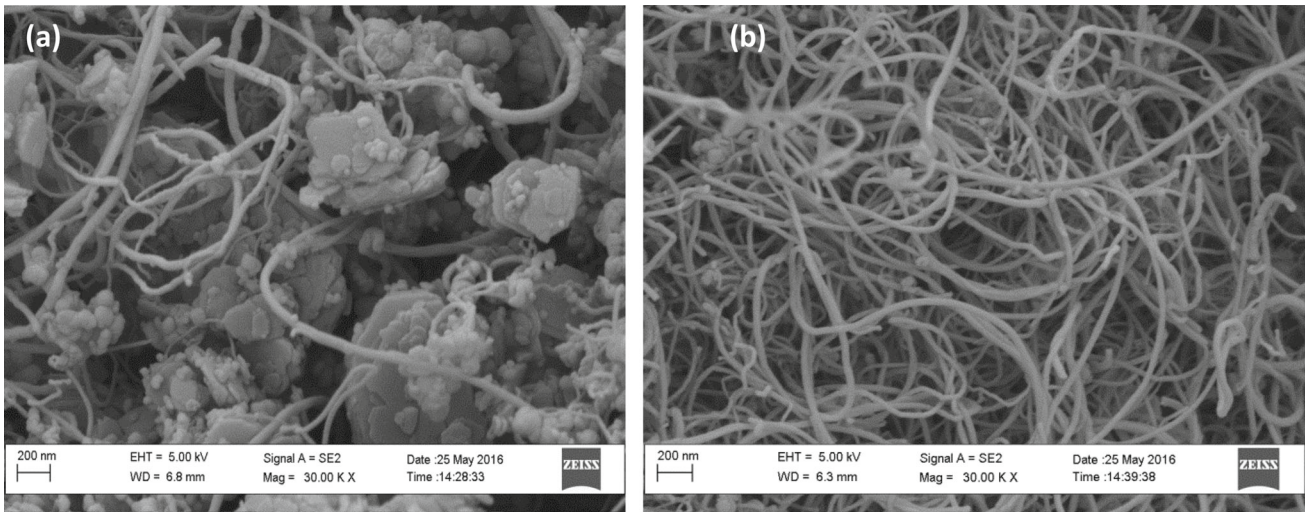

Fig. 1 HRSEM image of **a** as-produced CNF and **b** purified CNF

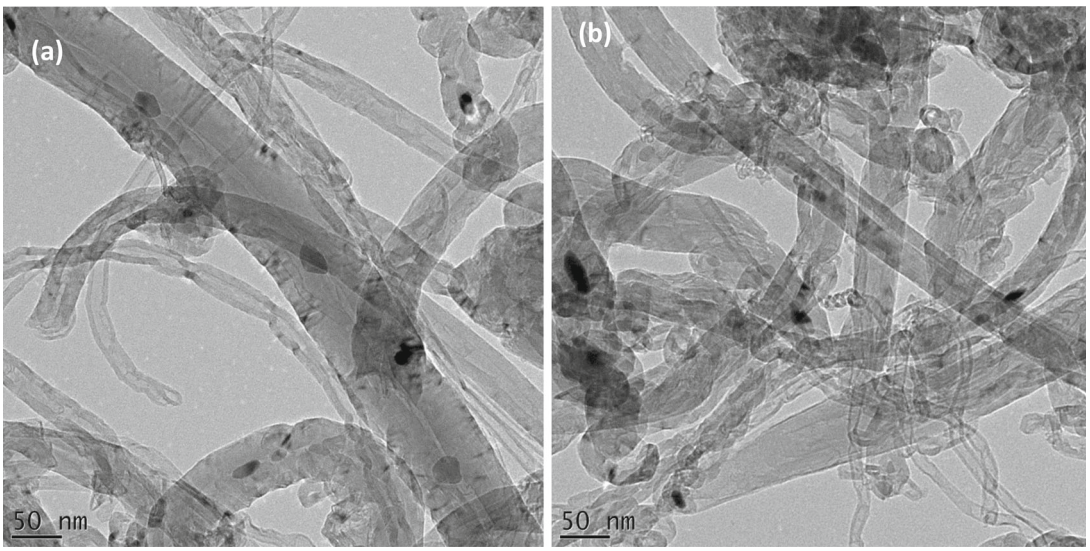

Fig. 2 **a** HRTEM image of as-produced CNF showing the internal and external fibre diameter **b** HRTEM image of purified CNF showing the deformation as a result of acid treatment

may be linked to the effectiveness of purification process. These results are in agreement with the study of Yehya et al. [23] that purification could lead to increase in surface area and consequently improvement in its catalytic activities.

The morphology and size distribution of as-produced and purified CNFs were examined using HRSEM, while the internal texture diameter and size distributions were measured by a HRTEM. The HRSEM images of as-produced and purified CNFs are presented in Fig. 1.

From Fig. 1, it can be noticed that the as-produced sample contains CNFs in a winding form surrounded by impurities from kaolin used as catalyst support. The micrograph also contains spread of Fe–Co catalyst nanoparticles which was used to promote the growth of CNFs in the CVD reactor. After acid treatment, the sample contains twisted form of CNFs with homogenous size entangled covered one another and grown both in length and diameter as observed in Fig. 1b. The growth both in length and diameter may be linked to the creation of functional groups onto the surface of the CNF. These functional groups facilitated the chemical interactions between the anchoring sites on the metal catalyst and the modified CNF. Though impurities in the form of amorphous carbon, metal catalyst as well as the support materials was still noticed in the purified catalyst, substantial parts of them were removed. Complete removal of the impurities cannot be achieved as this often leads to destruction of the fibre structure. Figure 2 shows the HRTEM micrograph of both as-produced and purified samples.

From Fig. 2, it can be seen that the nanofibers have inner diameter in the range of 19.5–40 nm. The outer diameter

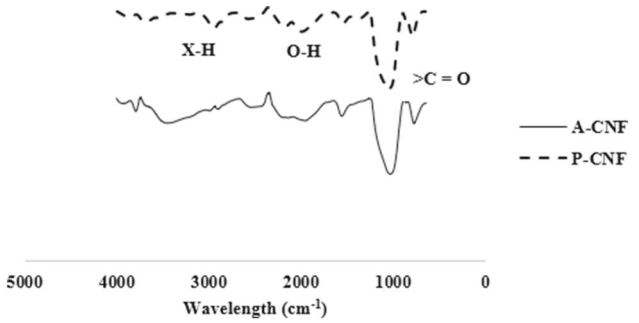

Fig. 3 FTIR spectrum of as-received and purified CNF

of CNF ranges between 25 and 100 nm which could be controlled by adjusting the synthesis time [24]. The image also showed that the diameter of purified CNF remains the same with as-produced CNFs, an indication that there was no significant change in spite of the acid treatment. Some metal particles were maintained at both the middle and the end of the fibres showing that the growth process probably followed the deposition diffusion–nucleation–growth mechanism [25]. The formation of metal particles at the middle of the fibres indicated that the support material (kaolin) which has several metal oxides had provided numerous active sites in which nucleation and subsequent growth of CNFs occurred. This observation contradicts tip or base growth mechanism observed with the use of other support materials such as alumina, silica and calcium carbonates [26]. However, during purification, it was observed that some deformations were formed on the fibres (see Fig. 2b). This deformation exhibited is one of the disadvantages of using acid treatments method for purification of CNFs.

The changes in the molecular structure of as-synthesized and purified CNF were studied using FTIR analysis. This was done to study the chemical bonding changes in the surface of the samples at a frequency range of 500–4000 cm^{-2}. The spectrum is presented in Fig. 3.

From Fig. 3, it was noticed that all the four regions in the mid-infrared spectrum were identified for both as-produced (A-CNF) and purified (P-CNF) CNF. Also, both spectra have all the fundamental vibrations in the 2500–4000 cm^{-1} due to the presence of O–H, C–H and N–H stretching in line with the observations of [27]. The band frequencies observed in the FTIR spectrum of both as-received and purified CNF are presented in Table 2.

From Table 2, it can be seen that the peaks at 1570 cm^{-1} correspond to the start of the carbonyl stretching and appeared at 1993 cm^{-1} on the purified CNFs and the broad stretch between 3477 and 3799 was assigned to O–H group. The carbonyl stretch observed may be due to free oxygen radicals produced during acid treatment which turned to oxygen atoms and later combined with the carbon atom to form the >C=O. This >C=O group joined with the –OH group of the same carbon atom to form –COOH [1, 23, 27]. The organic molecules such as the carboxylic, hydroxyl carbonic and sulphonic group were attached covalently to the CNFs. These are the functional groups that yielded the sites for attachment of substrates such as Pt ions which were subsequently reduced to Pt nanoparticles.

Table 2 The four regions of the mid-infrared spectrum (500–4000 cm^{-1})

Band frequency region	Identified band frequency for as-synthesized CNF	Identified band frequency for purified CNF
Finger print region (600–1500 cm^{-1})	707 and 1079	791 and 1000
Double bond region (1500–2000 cm^{-1})	1506 and 1991	1570 and 1993
Triple bond region (2000–2500 cm^{-1})	2384	2232
X–H stretching (2500–4000 cm^{-1})	2965 and 3726	2581, 3477 and 3799

2.8 Pt Catalyst Synthesis

Presented in Fig. 4a and b are the influence of mass of support (CNFs) and stirring time on the percentage of pt adsorbed onto the support.

The result as presented in Fig. 4a indicated that the Pt adsorption on CNFs increases from 20.94% using 0.25 g of CNF to about 76.27% using 0.3 g mass of CNFs. The increased higher surface provided for adsorption by CNFs which serves as support for Pt during synthesis. Also, as the mass of CNF increases, more active sites were available for adsorption and subsequent increase the nucleation of Pt nanoparticles. The adsorption sites were created by the CNFs support due to the presence of hydroxide ions impacted on it during acid purification treatment method. The nucleation was promoted by the reduction in bulk Pt to Pt nanoparticles by polyethylene glycol (PEG) during dispersion. The result obtained is in concordance with the findings of Seth et al. [8]. The mass of support (CNF) of 0.3 g which gave the highest percentage Pt (76.27%) was utilized to study the effect of deposition time on the amount of Pt adsorbed, and the result obtained is presented in Fig. 4b.

It can be deduced from the result shown in Fig. 4b that at stirring time of about 150 min, the percentage of Pt particle adsorbed by 0.3 g CNFs during catalyst preparation was found to be 80.38%. The result further revealed that when the stirring time was increased to 180 min, the amount of Pt adsorbed increases to about 80.94%. This showed that between 150 and 180 min, there was an effective stirring that enabled the creation of active sites for proper adsorption of Pt on the surface of the support. However, increase in stir-

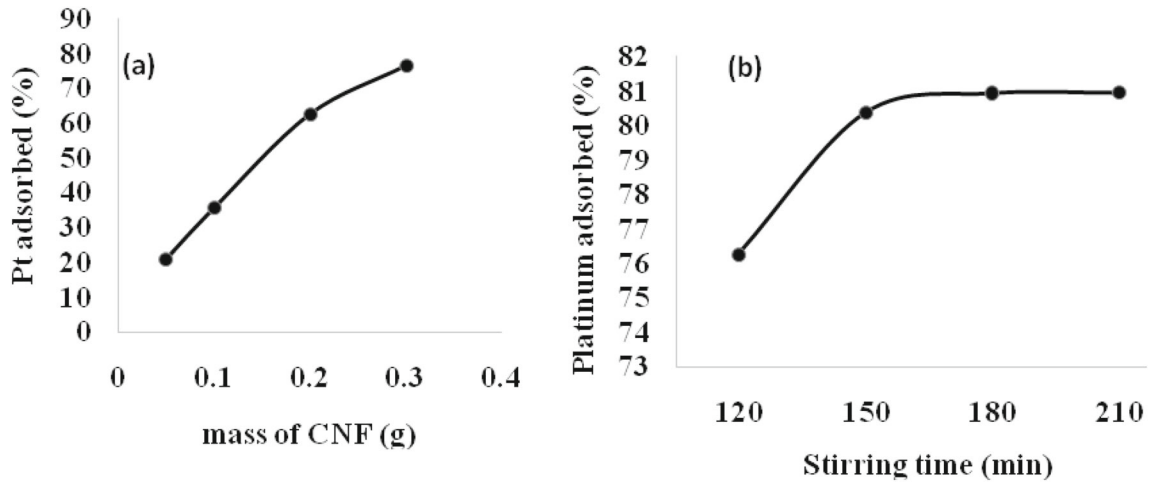

Fig. 4 Effect of **a** mass of CNF and **b** stirring time on Pt adsorption

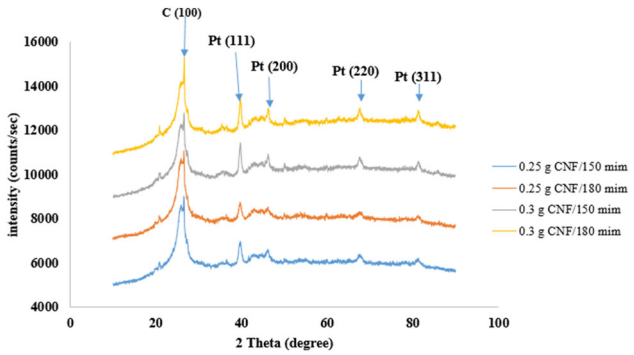

Fig. 5 XRD spectrum of CNFs/Pt catalyst

Table 3 XRD and TEM average crystallite size of the Pt catalyst and their crystallinity index

Pt synthesis conditions	XRD (nm)	TEM (nm)	Crystallinity index
0.25 g CNF/150 min	5.55	5.31	0.96
0.25 g CNF/180 min	5.54	5.50	0.97
0.3 g CNF/150 min	6.69	5.75	0.86
0.3 g CNF/180 min	5.57	5.88	1.06

ring time from 180 to 210 min revealed no further increase in the percentage of Pt adsorbed. This may be ascribed to the fact that at this time, the amount of CNF used during catalyst preparation has been saturated and there was no further space for adsorption of more Pt particle. The developed CNF/Pt catalyst was characterized to determine the crystalline nature using XRD, and the result is presented in Fig. 5.

From Fig. 5, the XRD patterns revealed five intense diffraction peaks at 2 theta values of 26.53°, 39.94°, 46.57°, 68.24° and 81.55°. The 2 theta of 26.53° with a corresponding crystal plane (100) depicts graphitic CNFs support. Other peaks identified showed the presence of a Pt structure at crystal planes of (111), (200), (220) and (311), respectively. This is in line with the work of other researchers such as afolabi [1], Aritonang et al. [3] and Prabhu [28], who independently reported formation of complex crystallite form of Pt nanoparticles. These spectra are indication that the Pt salt used in this work reduced to Pt atom in the form of nanoparticles. Another important information derived from the spectra in Fig. 5 is that the peaks became more sharper when 0.3 g mass of CNFs was used compared to 0.25 g CNFs support, which implies that more crystalline phase of Pt catalyst was synthesized with 0.3 g than 0.25 g. More so, small amount of support such as 0.25 g was not enough to absorb the available Pt concentration impregnated on it. However, irrespective of the stirring time, the Pt phases showed no differences in the diffraction pattern and this suggests that the lower stirring time (150 min) is enough for dispersion of Pt onto the matrix of CNFs at specified concentration of stabilizing agent (PEG). This is in agreement with the reported work of [1]. Average crystallite size of the catalyst was determined using Debby–Scherrer equation. The average crystallite size of Pt catalyst was between 5.54 and 6.69 nm. This is in close agreement with crystallite size obtained using HRTEM image (5.5–5.88 nm) as revealed in Table 3. The lattice parameter of the developed CNFs/Pt catalyst was calculated to be 3.902174Å.

Depicted in Fig. 6a–d are the HRTEM micrographs of the developed CNFs/Pt catalyst and their corresponding EDX. The HRTEM images revealed the presence of Pt nanoparticles scattered on the surface of CNFs. The presence of anchored Pt nanoparticles on the surface of CNFs was also confirmed by their respective EDX spectrum. The anchoring sites for adsorption of Pt nanoparticles were provided

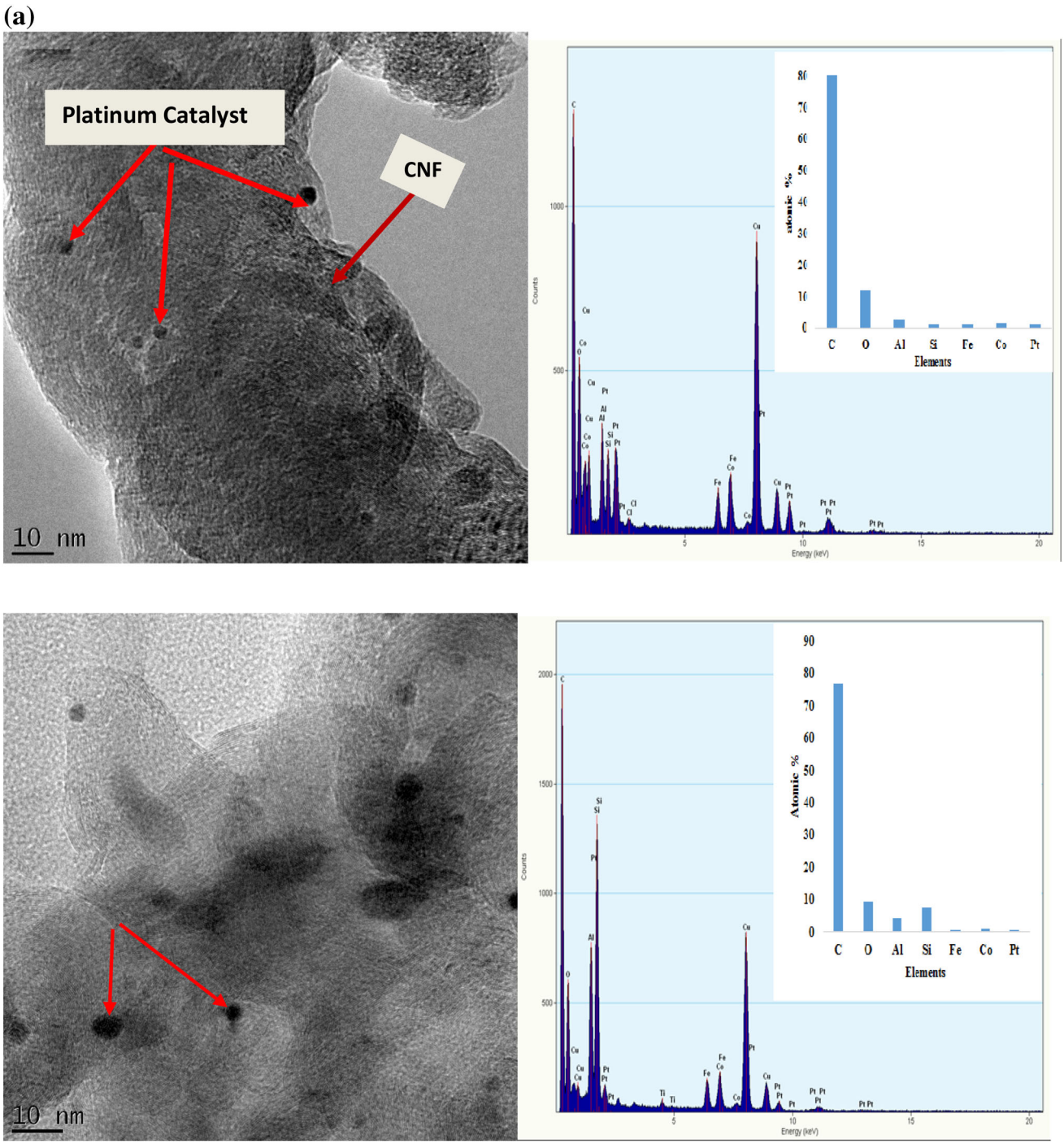

Fig. 6 **a** TEM images of CNF/ Pt catalyst and their corresponding EDX using 0.25 g CNFs. **b** TEM images of CNF/Pt catalyst and their corresponding EDX using 0.3 g CNFs

by the CNFs. This was as a result of introduction of functional groups such as hydroxyl and carboxylic group during the purification step. The EDX spectra also revealed trace amount of other elements such as cobalt, iron silica, aluminium and carbon. The presence of carbon indicates a graphitic nature of CNFs which serves as support and provides the anchoring sites for the Pt nanoparticles. Cobalt, iron, aluminium and silica are the traces of kaolin-supported Fe–Co catalyst used in the synthesis of CNFs.

However, the micrographs also revealed variations in the distribution pattern of Pt catalyst on the CNFs due to difference in the mass of support used during impregnation. Pt

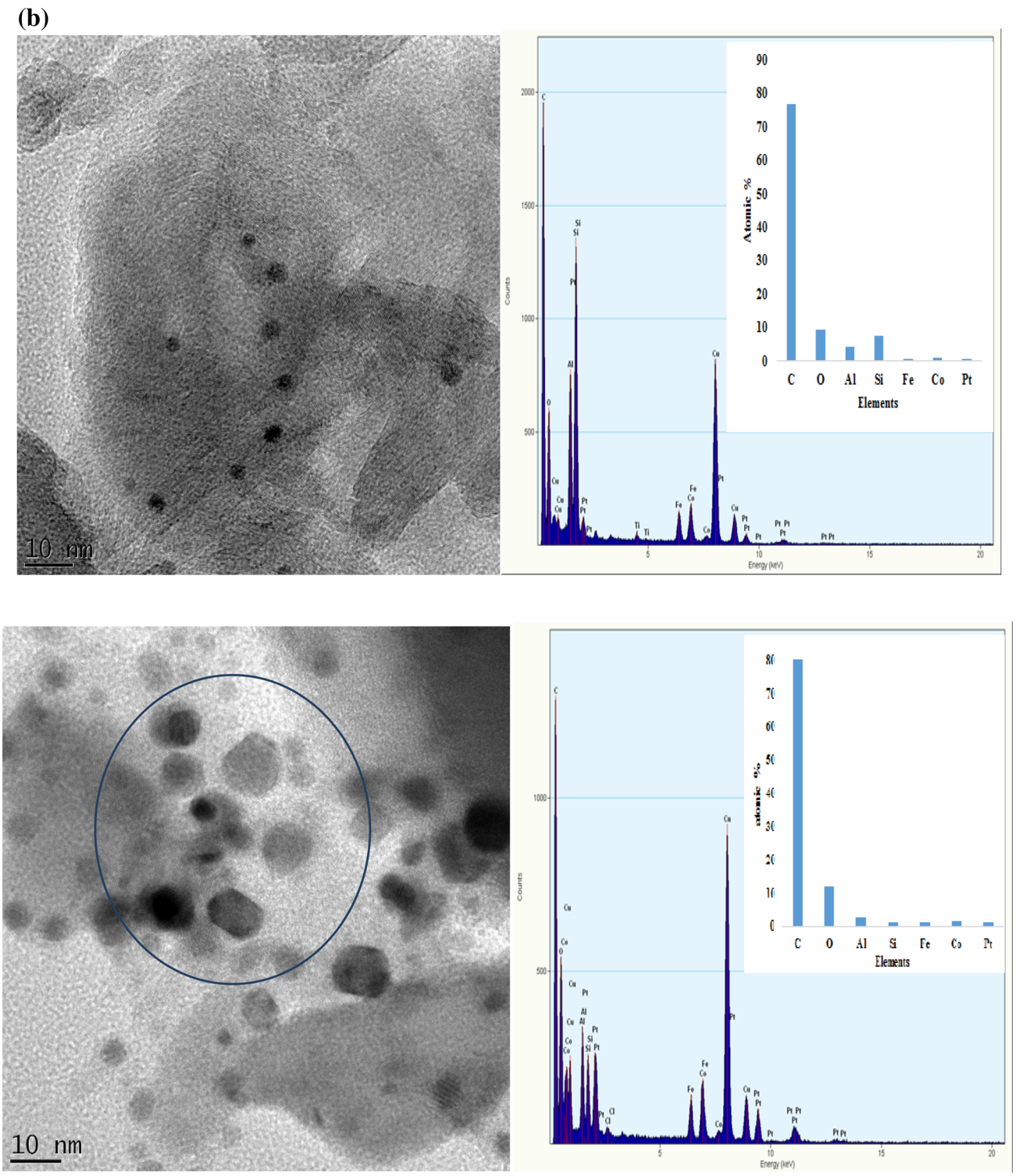

Fig. 6 continued

nanoparticles were sparsely distributed on CNFs using 0.25 g (Fig. 6a). The disparity in the nature of the distribution may be explained based on the fact that during impregnation, the Pt particles spread to occupy the space provided by 0.25 g of CNFs. Also, since the same amount of PEG was used for dispersion, more of the Pt was dispersed into the matrix of the CNF instead of onto the surface. In contrast, in Fig. 6b, Pt nanoparticles were more dispersed on the surface of the

CNFs because more of Pt particles were trapped at the surface when 0.3 g of CNFs used. This was attributed to higher quantity of carbon support requirements to match the concentration of Pt used during impregnation.

The Pt nanoparticles formed were of different shapes ranging from circular, rhombic, cubic and hexagonal (Fig. 6b). The shapes were as a result of polyhedral Pt nanoparticles brought about by better distribution into the matrix of CNF during synthesis [29]. The particle size distribution of Pt nanoparticles calculated ranges between 5.31 and 5.88 nm. This is in agreement with what is obtained as average crystallite size using Scherrer equation in XRD spectrum as presented in Table 3.

It has been reported that for nanoparticles of size less than 100 nm, there is tendency for the diffraction lines in XRD to be broad [30]. However, the peak breadth is a specific phase of Pt, and it is directly proportional to mean particle size of the material. It is also believed that sharp peaks denote crystalline materials [31]. It is therefore important to determine the crystallinity indices of the Pt nanoparticles to ascertain the type of crystals in the composites. The literature also revealed the relationship presented in Eq. (2).

$$I_{\text{cry}} = \frac{D_{\text{p}}(\text{SEM or TEM})}{D_{\text{cry}}(\text{XRD})} \text{ [32]} \tag{2}$$

where I_{cry} is the crystallinity index, D_{p} is the crystallite size obtained using TEM or SEM analysis, and D_{cry} is the crystallite size obtained using XRD.

The crystallinity index was determined, and the results are presented in Table 3.

From Table 3, it can be observed that the crystallinity index of synthesized sample using 0.25 g of CNF stirred for 180 min is 1.06. This implies that the Pt crystallites in the CNFs matrix are polycrystalline in nature and the structure is well indexed. Other calculated crystallinity indices are between 0.86 and 0.97. All these values are less than 1, an indicative of monocrystalline Pt in the matrix of CNFs. The monocrystallinity of the material may be linked to the complete reduction in Pt salt into its atom during impregnation wherein PEG performed dual roles of dispersant and reducing agent.

SAED patterns observed in all the samples tested are presented in Fig. 7. This is evidenced by the presence of sharp and bright diffraction rings. The brightness of the rings connotes the polycrystalline Pt nanoparticles. This is in agreement with the result of crystallinity index. Each ring in the SAED pattern represents the diffraction from crystals of almost the same size. A noticeable bright spot in the pattern corresponds to each diffraction peak in XRD pattern..

From Fig. 7, the visible (d_{hkl}) indices for Pt nanoparticles were (111), (200), (220) and (311). These correspond to diffraction angles of 39.91°, 46.43°, 67.76° and 81.69° respectively. However, from Fig. 7a and b, it was observed that only the planes (200) and (220) rings were prominent. This corresponds to diffraction angles of 46.98° and 69.80°, respectively. Figure 7c reveals the planes (200) and (311) with corresponding diffraction angles of 46.47° and 84.72°, respectively, while that of Fig. 7d shows only plane (311) at a diffraction angle of 84.28°. These peaks are in good agreement with the peaks assigned in XRD data. This implies the presence of highly crystalline Pt nanoparticles. This result is in line with the works of Viet-Long et al. [29] who also reported the presence of these planes for a typical face cubic centre of Pt nanoparticles. The interplanar spacing (d) as a function of the Miller indices and the length between two bright spots in the SAED patterns were determined. The reciprocal interplanar spacing ($1/d$) was calculated using the pronounced peaks shown in SAED patterns of Fig. 7. The result of the interplanar spacing as a function of the miller indices is presented in Table 4.

According to Table 4, the d-spacing of the Pt nanoparticle's crystals of planes (200) was 0.195 and 0.227 for samples synthesized with 0.25 g of CNFs (0.25 g) stirred for 150 min and 180 min, respectively. This indicated mixture of polyhedral facet and cubic shaped Pt nanoparticles, respectively. Other lattice fringes such as (220) and (311) d-spacing occurred within the ranges of 0.107–0.196. This can be linked to the presence of hexagonal structured octahedral, and tetrahedral or truncated cubic, octahedral and tetrahedral. The difference in d_{hkl} of the Pt crystals synthesized at different conditions was ascribed to different shapes of Pt nanoparticles in the catalyst [29].

XPS analysis was used to determine the chemical state composition of Pt nanoparticles as well as the nature of Pt compound present. The full spectrum for the catalyst showing its elemental composition is presented in Fig. 8, while the spectrum for the Pt core level states is presented in Fig. 9.

In Fig. 8, carbon and oxygen remain the dominant elements. The carbon at the binding energy of 284.5 eV corresponds to graphitic CNFs used as a support for the Pt catalyst during impregnation. Other elements identified include O (1s), Ar and Si as well as a very low concentration of Pt. The O1s and O KLL are the main peak and auger peak of oxygen in the sample, respectively. The O1s is the photoelectron line that was observed as a peak after sputtering, while the O KLL was formed at a K and double L vacant shell in the form of oxygen peak after sputtering. The binding energies of both O (1s) and O KLL are 533 eV and 744 eV, respectively. The presence of argon (Ar) was as a result of the Ar ion beam used for sputtering. Si (2s), Si (2p) originated from the kaolin used for the CNFs synthesis. Si peak appeared as a major peak because it was released as free element during heat treatment of CNF growth.

Figure 9 reveals the presence of two chemical states of Pt with an overlapping region of Al 2p. The two peaks cor-

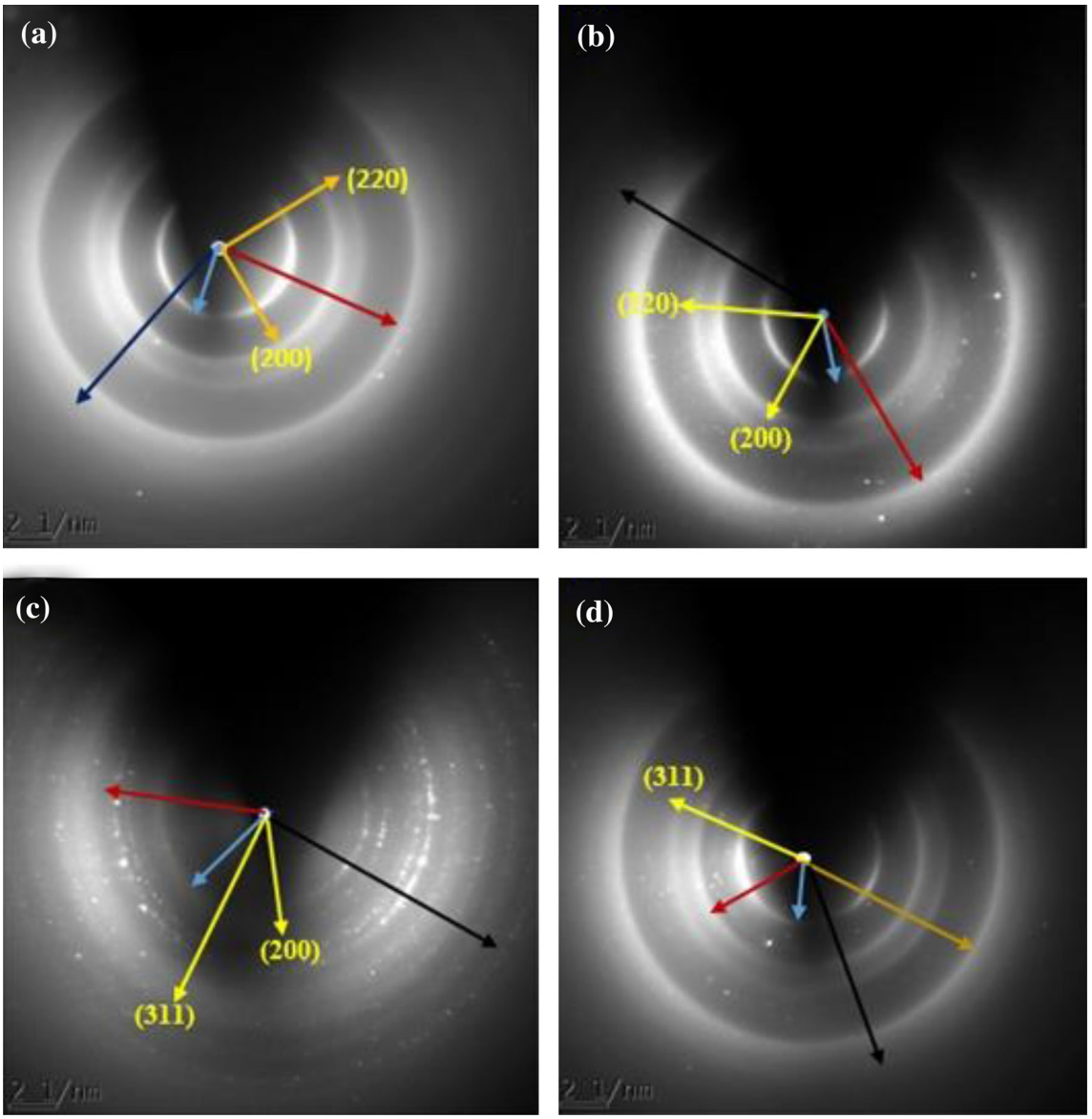

Fig. 7 SAED patterns of the CNF/Pt catalyst **a** at (200) and (220) for 0.25 g CNF/150 min. **b** At (200) and (220) for 0.25 g CNF/180 min. **c** (200) and (311) for 0.3 g CNF/150 min. **d** At (311) for 0.3 g CNF/180 min

Table 4 Phase identification for Pt catalyst in SAED pattern

Pt-CNF catalyst samples	*h*,*k*,*l*	d_{hkl} (nm)	$1/d_{hkl}$ (nm^{-1})
0.25 g CNF/150 min	200	0.195	5.128
	220	0.138	7.246
0.25 g CNF/180 min	200	0.227	4.405
	220	0.196	5.102
0.3 g CNF/150 min	220	0.169	5.917
	311	0.107	9.346
0.3 g CNF/180 min	311	0.154	6.494

respond to Pt $4f_{7/2}$ and $4f_{5/2}$ orbital, respectively, while the overlapping of the presence of aluminium originated from the kaolin used as support for the bimetallic catalyst employed for synthesis of CNFs. The relatively flat background on the higher binding energy side indicates Pt in the surface atomic layer. The Pt 4*f*-A represents Pt $4f_{7/2}$ at binding energies of 71.125 eV and 75.5 eV. The Pt 4*f*-B denotes Pt $4f_{5/2}$ at binding energies of 74.5 eV and 77.5 eV. According to XPS reference table of elements, 71.0 eV is used to identify the chemical state of atomic Pt [33]. However, it was noted that the chemical states of all the Pt peaks fall above 71.0 eV. This is an indication that the Pt salt used in this study did not undergo complete reduction into Pt atom, rather a compound of Pt was formed.

It is obvious from Table 5 that the Pt exists in the catalyst in the following forms: Pt_2Si, Pt $(OH)_2$, Pt oxides, Pt Cl_4 and

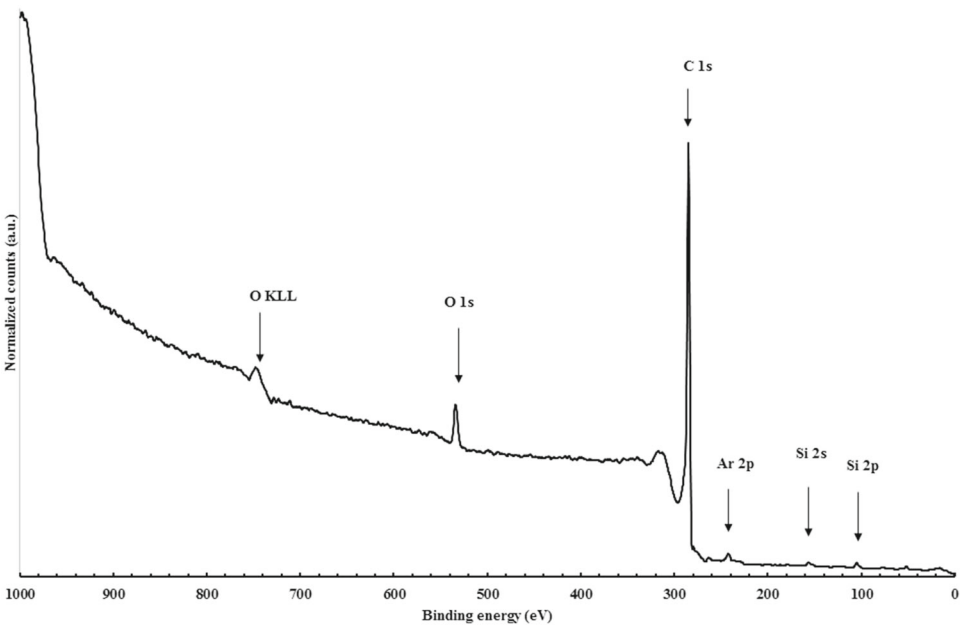

Fig. 8 XPS general survey of CNFs/Pt catalyst

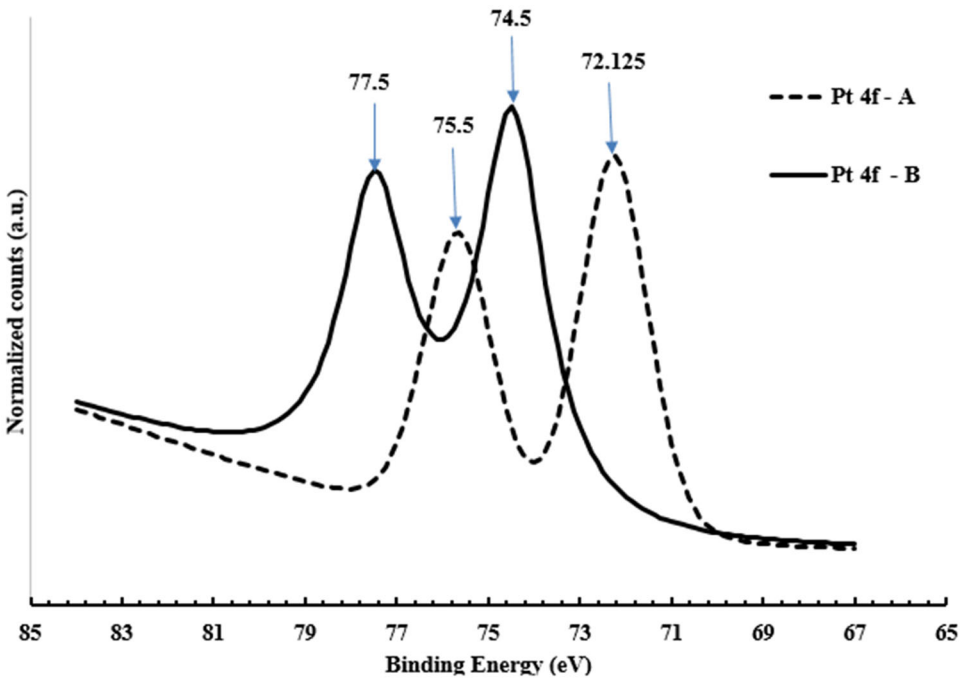

Fig. 9 The spectrum of Pt 4f core level in the catalyst

Pt(IV) halides. For instance, Pt $(OH)_2$ detected was linked to the reaction of hydroxyl functional groups in the PEG with Pt, while the oxide formation of Pt oxides was due to the presence of polyethylene oxide. Also, during impregnation of Pt nanoparticles by ethylene glycol method, the metallic Pt on the surface of the support formed intermediate product and remains unreduced to Pt $(OH)_2$. The presence of silica as an halide attached to Pt atom to form Pt_2Si was as a result of free silica generated during dehydroxylation of kaolin in the synthesis of Fe–Co/kaolin catalyst used for the growth of CNFs. $PtCl_4$ was derived from the compound of Pt (K_2PtCl_4) precursor used for the catalyst synthesis, while Pt(IV) halides were formed due to the reaction with the chlorine in the parent sample of Pt used in this study.

The TGA profiles of CNFs and CNFs/Pt catalyst are presented in Fig. 10. It can be noticed that the purified CNFs exhibited about 83% decomposition in air at a temperature of about 467 °C. This indicated a characteristic curve of a crystalline carbon showing little or no presence of impurities in the form of metal particles and amorphous carbon. In contrast, slight changes were observed at temperature between 400 and 420 °C for all the Pt-CNF catalysts. This indicated

Table 5 Pt compounds formed and their binding energy

Binding energy (eV)	Compound
72.125	Pt_2Si, $Pt(OH)_2$
74.5	Pt oxides
75.5	$PtCl_4$
77.5	Pt (iv) halides

that the Pt salt used reduced at standard reducing temperatures as reported by Afolabi [1].

However, the difference between these curves and that of purified CNF depicted the amount of Pt impregnated on the CNF. The purified CNF sample was stable up to a temperature of about 600 °C, while all Pt-CNF samples were stable to a temperature of between 500 and 550 °C (Fig. 10). The differences in stability may be attributed to the presence of Pt particles in the latter and not in the former. This temperature is far higher than the working temperature of low-temperature fuel cell, which is in the ranges of 60–100 °C [2].

2.9 Electrochemical Measurement of CNFs/Pt Catalyst

The electrochemical activity of the synthesized catalysts was carried out using cyclic voltammetry (CV) technique to determine the specific and mass activity of the catalyst. The CV was carried out by cycling the potential between two points, while currents generated were recorded. These currents represent the anodic and cathodic reactions in the fuel cell. The results of CV of Pt catalyst are presented in Figs. 11 and 12. Figure 11a and b shows the cyclic voltammogram of Pt catalyst obtained using 0.30 g CNFs at a deposition times of 150 min and 180 min, respectively. From the CV, the oxidation and reduction areas represent the charge amount of the hydrogen electrodesorption on Pt.

As shown in Fig. 11a, the negative direction of potentials of between 0.8 and − 1.8 V implies no visible peaks and this corresponds to hydrogen evolution. On the other hand, adsorption of hydrogen onto the Pt surface was observed around the potentials of − 0.5 and − 0.3 V. The subsequent higher potentials represent oxide reduction and formation. This imply that hydrogen oxidation reaction (HOR) currents were noticed, but partial oxygen reduction reaction (ORR) current occurred over the potential ranges studied. However, the actual Pt reduction began at a potential of − 0.2 V, showing a single peak with no oxidation currents observed during scanning. This invariably means that the sample exhibited electrocatalytic activity for HOR. The result as presented in Fig. 11b revealed that adsorption of hydrogen onto the Pt surface was observed around the potentials of − 0.8 and − 0.3 V. The figure also shows no peak attributed to ORR. The reason for the similarity in Fig. 11a and b could be traced to the same amount of Pt used during the deposition process as well as same mass of CNFs but at different deposition times. The variation in deposition time has no effect on the catalytic activity of the catalysts.

Figure 12a shows the CV of catalyst synthesized using 0.25 g CNFs deposited on Pt surface for 150 min, while Fig. 12b shows the voltammogram of catalyst synthesized using the same amount of CNF but deposited for 180 min.

The result as presented in Fig. 12 showed that the peaks for hydrogen evolution, adsorption and desorption were partially revealed at potentials of between − 0.4 and − 0.3 V, while peaks corresponding to Pt oxide formation and reduction were observed at potentials of between higher potentials

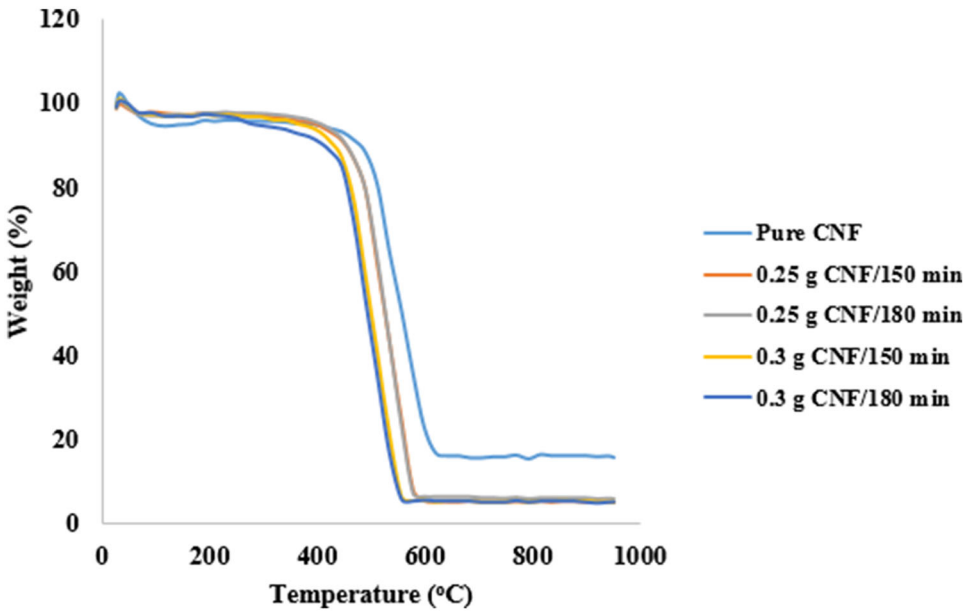

Fig. 10 TGA spectrum of CNF/Pt catalyst

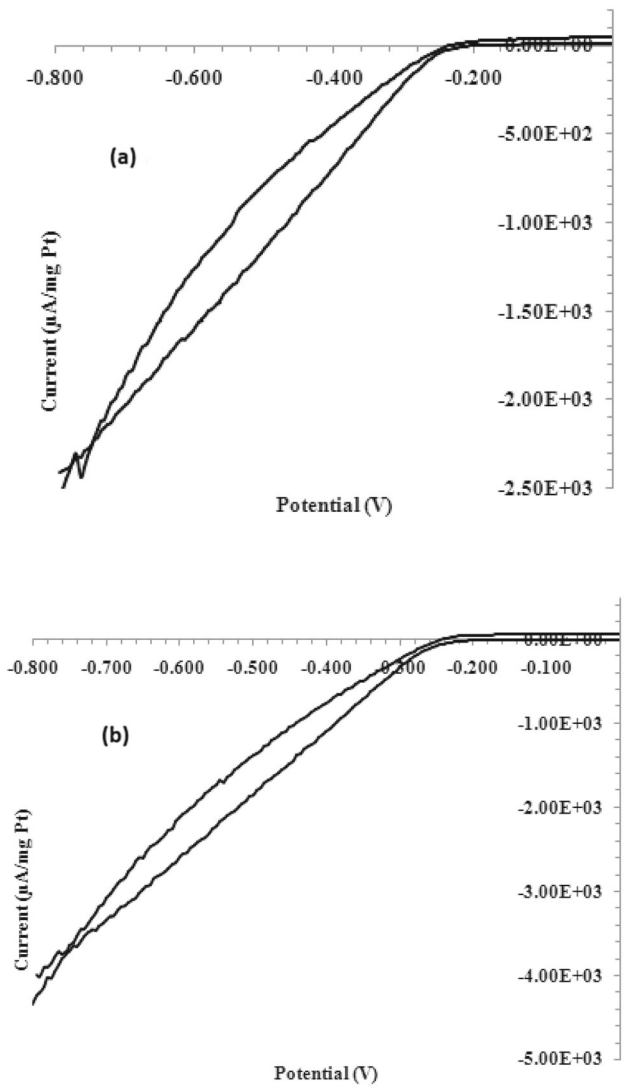

Fig. 11 Cyclic voltammogram of 0.30 g Pt catalyst at deposition time of **a** 180 min, **b** 150 min at a scan rate of 20 mV/s in nitrogen-saturated 0.5 M H_2SO_4

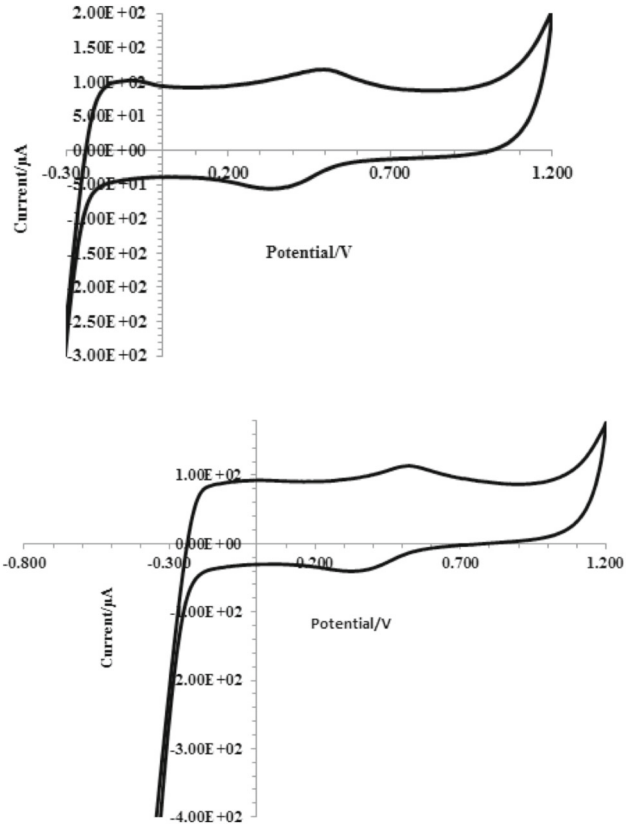

Fig. 12 Cyclic voltammogram of 0.25 g Pt catalyst at deposition time of **a** 180 min, **b** 150 min at a scan rate of 20 mV/s in nitrogen-saturated 0.5 M H_2SO_4

of − 0.2 and 1.2 V. The difference between these voltage ranges using 0.3 g Pt catalyst was because at these potentials, the electrochemical activities of this catalyst were more pronounced and the performance of the electrodes was easily captured. These correspond to peak current density of around 0.014 A/mg Pt. This implies that ORR activity was observed in the catalyst. The evidence of the presence of ORR current could be ascribed to the shape of the voltammogram owing to the increasing inert gas purge rate during scanning. When this occurs, there was possibility of hydrogen being swept away from the electrode surface thereby decreasing its partial pressure. For instance, Jäger et al. [34] revealed that when the partial pressure of hydrogen reduced, the possibility of increasing in reversible potential for hydrogen evolution is high. This usually caused difficulty in quantifying the hydrogen adsorption from the voltammogram, and by extension formation of oxide and occurrence of reduction. Also, the shape as shown in the figure suggested the presence of approximately about 20% Pt oxide as confirmed by XPS analysis. However, the shape of cyclic voltammogram in Ar-saturated 0.5 M H_2SO_4 solution depends slightly on the Pt. Also, the shape connotes the incomplete reduction in Pt salt in the form of PtO. This shows that the small Pt loading and small amount of CNF used as support in this study support ORR kinetics. The result as presented in Fig. 12b also revealed partial hydrogen evolution and adsorption between the potentials of − 0.5 and − 0.3 V. This implies that the voltammogram of 0.25 g CNF-supported catalyst synthesized at deposition time of 180 min partially supported HOR activity. However, at higher potentials of between − 0.2 and 1.2 V, the peaks corresponding to Pt adsorption and subsequent formation of its oxide were revealed. This shows that ORR activity is supported by the catalyst. This corresponds to a current density of about 0.016 A/mg Pt.

The electrochemical active surface area (ECSA), catalyst utilization and roughness factor of the Pt catalyst were calculated from the voltammogram, and the result is presented in Table 6.

Table 6 ECSA, catalyst utilization and effective roughness factors obtained from the CV of synthesized Pt catalyst

Catalyst synthesis conditions	ECSA (m^2/g)	Catalyst utilization (%)	Roughness factor
0.25 g CNFs/150 min	125.90	31.65	68.64
0.25 g CNFs/180 min	84.80	25.58	51.84
0.3 g CNFs/150 min	141.86	38.19	75.58
0.3 g CNFs/180 min	166.14	37.61	98.04

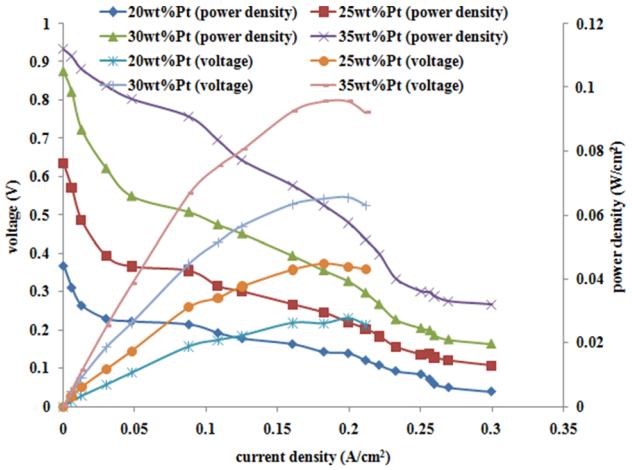

Fig. 13 Polarization curve of a single cell operated at 25 °C with H_2/O_2 ratio of 1:2

Table 6 reveals availability of higher active surface area for reactions (ECSA) with catalyst synthesized using 0.30 g CNF as compared to those synthesized using 0.25 g CNFs. This higher ECSA may be attributed to partial hydrogen adsorption and desorption peaks obtained during cyclic voltammetry experiment leading to longer ORR activities. Also, there may be lower aggregation of Pt nanoparticles on CNFs due to deactivation after potential cycling. This result corroborates the findings of Yu-chun et al. [35] who attributed higher ECSA to the scattered and non-agglomeration nature of metallic nanoparticles on the support. This is evidenced from the HRTEM characterization results. The lower ECSA attributed to catalyst synthesized with 0.3 g CNFs may be due to loss of Pt owing to support porosity and eventual blockage of mass transfer pathways. This result is in line with the reported observations of Farokh et al. [36]. The authors found that lower ECSA may be due to Pt loss or crystal merging due to collapse of carbon support. However, the increase in ECSA noticed as a result of increase in mass of CNF from 0.25 to 0.30 g was due to an improvement in particle dispersion, as well as reduction in particle size as confirmed by XRD and TEM results. The dispersion time variation from 150 min to 180 min showed no specific pattern because both dispersion times used were sufficient for proper dispersion of Pt on the surface of CNF and reduction in complexity of nucleation process induced by the PEG.

From Table 6, it can be seen that about 37.61 and 38.19% of the catalyst were utilized by 0.30 g CNFs-supported catalyst as against 25.58 and 31.65% catalyst utilization by 0.25 g CNF-supported catalyst. This may be associated with the larger surface area created by the porosity of the catalyst and no loss of Pt nanoparticles during the process. Also, since CNFs are not liable to corrosion in comparison with carbon black, mass transfer pathways were enlarged, and triple phase boundary was created, hence more catalyst utilized. The roughness factors showed that dispersion of Pt nanoparticles onto the pores of the support took place. This result is in agreement with the outcome of Noramalina [2] who observed that for a well-dispersed polycrystalline Pt nanoparticle, the roughness factor of carbon-supported catalyst ranged between 1 and 10^5. However, according to [37], for a typical Pt electrodes, the roughness factor should be 2, although higher values were obtained in this study. This might be attributed to leakage through the Pt and glass electrodes as a result of diffusion of water along Pt/glass boundary leading to the formation of an aqueous film that covers the Pt wire.

The performance of the developed electrodes (CNFs/Pt composite) was evaluated through influence of catalyst loading on the fuel cell performance. Depicted in Fig. 13 is the polarization curve of the influence of catalyst loading on the cell performance at constant fuel/oxidant ratio (1:2), operating temperature (25 °C), operating pressure (1 bar) and humidity (50%).

Figure 13 shows an increase in current density leads to a drop in cell voltage irrespective of the catalyst loading. This can be linked to the well distribution of platinum nanoparticles on the CNF-supported matrix which aided the transportation of electrons within the electrodes. This result is in line with the observations of Afolabi [1]. The author opined support material such as the CNF has the ability to transport electrons from the anode to the cathode via the current collectors of the fuel cell. This can lead to lower voltage drops across the cell. High surface areas of the CNFs can also be responsible for this observation.

Figure 13 also reveals an increase in the open-circuit voltage (OCV) of the fuel cell with increase in catalyst loading. For instance, the OCV of the fuel cell of 20, 25, 30 and 35 wt% Pt catalysts loading was 0.36, 0.63, 0.88 and 0.93 V, respectively. However, the obtained OCVs of the electrode of the fuel cell deviated from the standard OCV of PEMFC at standard conditions (1.2 V). These differences may be ascribed to the overpotentials induced during the MEA fabrication.

Table 7 Characteristics of the fabricated electrode

Electrode sample (wt% Pt)	Open-circuit voltage (V)	Power density (W/cm^2)	Exchange current density (A/cm^2)	Pt catalyst loading (mg_{Pt}/cm^2)	Mass activity (A/g)	Tafel constant
20	0.369	0.028	2.44	0.002	0.3	0.8821
25	0.635	0.045	2.42	0.003	0.3	1.4788
30	0.876	0.066	2.41	0.003	0.4	2.1556
35	0.934	0.095	2.31	0.004	0.4	2.3865

Large voltage drop also occurred at low current density due to slow kinetics of ORR at the cathode of the cell. This is because, at low current densities, slow kinetics of ORR is the controlling factor that leads to low voltage drop and hence slow performance of the fuel cell.

Generally from Fig. 13, there was an increase in cell voltage at higher current densities with increase in catalyst loading. This shows that the performance of the electrodes of the cell increases with increase in catalyst loading when fabricated using the same process and operated at the same operating conditions. The higher performance at higher loadings may be connected with the smaller particle size of the platinum in the catalyst with low agglomeration as evidenced in HRTEM results. The power density of the electrodes as a function of the current density shown in Fig. 13 also confirmed that an increase in catalyst loading resulted in an increase in power density of the fuel cell. Thus, the maximum power density of electrodes fabricated with catalyst loading of 20 wt% Pt increases from 0.027 to 0.095 W/cm^2 for electrode fabricated with 35 wt% platinum catalyst loading. This also indicated that the performance of the electrodes increases with increase in platinum loadings. This may be connected with the ability of platinum catalyst to promote electrochemical reactions. The general characteristics of the developed electrode in a fuel cell were evaluated with the aid of Tafel equation, and the result is presented in Table 7.

According to Table 7, it is obvious that the amount of Pt catalyst in the electrode sample increases from 20 wt% Pt to 35 wt% Pt, and the open-circuit voltage (OCV) increases from 0.369 to 0.934 V. This implies that the high surface areas CNFs as shown in BET analysis result of Table 1 created more active sites for homogenous distribution of Pt catalyst in the MEA for electrochemical reactions to take place at the electrodes of the fuel cell. This is an evidence of direct proportional relationship between reaction kinetics at the electrodes and voltage generated by Tafel equation. The table also revealed that an increase in open-circuit voltage (OCV) caused an increase in power density from 0.028 to 0.095 W/cm^2. The increase in OCV might be attributed to no crossover current at this point due to its lower value, and hence, the resistance to flow of current was felt by the supporting material yielding high OCV. It has been reported that when the cell voltage is not corrected at its initial stage due to crossover current, there may be loss of voltage and can be otherwise led to high OCV [38].

It can also be seen from Table 7 that the values of Tafel constant increase from 0.8821 to 2.3865 as the amount of Pt catalyst in the electrode sample increases from 20 to 35 wt%. At low Tafel constant, electron transfer pathways reduced due to sluggish reaction mechanism. With increased Tafel constant, the mechanism of reaction improves due to change in oxygen reaction pathways caused by loss in mass transport posed to the Pt electrode by the CNFs particles. This resulted into increase in mass activity of the electrode from 0.3 to 0.4 A/g. This result is in tandem with the report of Shukla [38], Liang et al. [39], Rashmi et al. [40] and Morawietz et al. [41]. However, as presented in Table 7, it could be seen that as the amount of Pt catalyst in the electrode increased from 20 to 35 wt%, the exchange current density decreases from 2.44 to 2.31 A/cm^2. The decrease in exchange current density was a result of polarization that occurred in the cell owing to ohmic losses during MEA fabrication. This occurrence of ohmic losses may be due to resistance posed by the electrolytes and the electrodes in fuel cell. The effects of these losses were mostly pronounced at intermediate current densities of between 1 and 5 A cm^{-2} [2].

The increase in the amount of Pt catalyst in the electrode samples and increase in the Pt catalyst loadings (the amount of Pt catalyst that actually participated in the electrochemical reaction) as observed in Table 7 may be explained as follows. The CNFs provided more space for anchoring of the Pt nanoparticles due to its high surface area which is considered a necessity for the good development for the electrode of the fuel cell. Not only that, the reduction in Pt loading resulted in decrease in the resistance of the passage of electrons in the electrode and at the same time increase in the electrochemical active surface area (ECSA). This in turn allows for influx of oxygen through the membrane film to the catalyst site. At the site, the oxygen eventually reacted with the incoming hydrogen to form water as one of the by-products. Also, water management of the membrane was improved thereby increasing the efficiency of the electrode yielding high performance. The result of Pt catalyst loading from this research

Table 8 Pt loadings of reference catalyst

Electrocatalyst type	Pt loading (mg_{pt}/cm^2)	Open-circuit voltage (V)	References
Pt–C	0.1	0.95	[42]
Pt–CNT	0.06	0.90	[43]
Pt–Ti	0.038	0.89	[44]
Pt–AuC	0.04	0.946	[45]
Pt–SiC	0.2	0.90	[46]
Pt–xerogel	0.4	0.964	[5]
Pt–C	0.05	0.90	[41]
Pt–C	0.2	0.80	[47]
Pt–CNFs	0.004	0.934	This study

showed an improvement compared to other catalyst support materials as presented in Table 8.

3 Conclusions

CNFs/Pt catalyst was successfully synthesized from precursor solution of K_2PtCl_4, Fe-Co/kaolin by combination of chemical vapour deposition and wet impregnation method. The variation of dosage of CNFs and deposition time influenced the stability, microstructures, crystalline and oxidation states of Pt on the surface of CNFs. The particle size, shapes and morphology of the catalyst were affected by the mass of CNF (0.25 g and 0.3 g) used and, however, independent of the stirring times between 150 and 180 min. The catalyst was stable to a temperature of about 500 °C and 550 °C and can withstand the working temperature of a low-temperature PEM fuel cell. The XPS analysis revealed that the synthesized catalyst was of two chemical states at binding energies of between 71.125 and 77.5 eV, an indication that the catalyst exists as compound. The electrochemical measurement of the catalyst by cyclic voltammetry revealed that the catalyst developed supported both ORR and HOR in the fuel cell. Performance evaluation of the fuel cell using the MEA fabricated from the electrode showed that the Pt loading of the developed electrode from this research showed an improvement compared to other catalyst support materials.

Acknowledgements This is to acknowledge and appreciate the support received from the Tertiary Education Trust Fund (TETFUND) of Nigeria under grant number TETFUND/FUTMINNA/2017/09. The authors also thank The Centre for Genetic Engineering and Biotechnology (CGEB) FUTMinna who offered us direct access to their facilities. We are also grateful to the following people that helped analysed the samples: Dr. Remy Bucher, (iThemba Labs), Cape Town, South Africa, for XRD, Dr.Franscious Cummings, Electron Microscope Unit (EMU), Physics Department, University of Western Cape (UWC), South Africa, for HRTEM. Adrian Joseph, Physics department, UWC, South Africa, for HRSEM and Prof. W.D Roos, Physics Department, University of the Free State, South Africa, for XPS.

References

1. Afolabi, A.S.: Development of Pt electro catalytic electrodes for proton exchange membrane fuel cell. PhD Thesis, University of the Witwatersrand, Johannesburg, pp. 115–142 (2009)
2. Noramalina B.M.: Development of catalysts and catalyst supports for polymer electrolyte fuel cells. Ph.D Thesis, University College, London, Torrington, London, pp. 25–38 (2014)
3. Aritonang, H.F.; Onggo, D.; Ciptati, C.; Radiman, C.L.: Synthesis of Pt nanoparticles from K_2PtCl_4 solution using bacterial cellulose matrix. J. Nanoparticles (2014). https://doi.org/10.1155/2014/285954
4. Oliver, T.H.; Joseph, W.S.: The role of Pt in proton exchange membrane fuel cells. J. Pt Metals Rev. **57**(4), 259–271 (2013). https://doi.org/10.1595/147106713X671222
5. Cinthia, A.; María, E.G.; Rafael, M.; María, J.L.: Influence of the synthesis method for Pt catalysts supported on highly mesoporous carbon xerogel and vulcan carbon black on the electro-oxidation of methanol. Catal. J. **5**, 392–405 (2015). https://doi.org/10.3390/catal5010392
6. Rabis, A.; Rodriguez, P.; Schmidt, T.J.: Electrocatalysis for polymer electrolyte fuel cells: recent achievements and future challenges. ACS Catal. J. **2**, 864–890 (2012)
7. David, S.; Isabel, S.; Rafael, M.; María, J.; Lázaro, A.S.; Vincenzo, B.; Antonino, S.A.: Optimizing the synthesis of carbon nanofiber based electrocatalysts for fuel cells. Appl. Catal. B J. Environ. **132–133**, 22–27 (2013)
8. Seth, L.K.; Wenzhen, L.; Odysseas, P.; Thomas, M.M.; Jeremy, S.; Pradeep, H.: The effect of experimental parameters on the synthesis of carbon nanotube/nanofiber supported Pt by polyol processing techniques. Carbon J. **46**, 1276–1284 (2008)
9. Li, W.; Mahesh, W.; Zhongwei, C.; Paul, L.; Yushan, Y.: Pt nanopaticles supported on stacked-cup carbon nanofibers as electrocatalysts for proton exchange membrane fuel cell. Carbon J. **48**, 995–1003 (2010)
10. Iuliia, M.: Synthesis and characterisation of nanofibre supports for pt as electrodes for polymer electrolyte fuel cells. PhD Thesis, University of Montpellier, Montpellier (2014)
11. Sergey, A.G.; Vladimir, N.F.; Elena, K.L.; Alexander, S.G.; Dmitri, G.B.; Xing, W.; Junjie, G.: CNF-supported Pt electrocatalysts synthesized using plasma-assisted sputtering in pulse conditions for the application in a high-temperature PEM fuel cell. Int. J. Electrochem. Sci. **11**, 2085–2096 (2016)
12. Hyung-Suk, O.; Jong-Gil, O.; Hansung, K.: Modification of polyol process for synthesis of highly Pt loaded Pt–carbon catalysts for fuel cells. J. Power Sources **183**, 600–603 (2008)
13. Zhang, Y.; Dafei, K.; Carl, S.; Mark, A.; Can, E.: Supported Pt nanoparticles by supercritical deposition. Ind. Eng. Chem. Resour. **44**, 4161–4164 (2005). https://doi.org/10.1021/ie050345w
14. Sajid, H.; Heiki, E.; Nadezda, K.; Maido, M.; Mihkel, R.; Väino, S.; Gilberto, M.; Kaido, T.: Pt particles electrochemically deposited on multiwalled carbon nanotubes for oxygen reduction reaction in acid media. J. Electrochem. Soc. **164**(9), F1014–F1021 (2017)
15. Roxana, M.; Dragoș-Toader, P.; Gabriela, M.; Nicolae, V.; Nicolae, V.: Carbon nanofibers decorated with Pt–Co alloy nanoparticles as catalysts for electrochemical cell applications synthesis and structural characterization. Int. J. Electrochem. Sci. **12**, 4597–4609 (2017). https://doi.org/10.20964/2017.05.25
16. Aminul, I.M.; Anwarul, K.B.; Saidul, I.M.: A review on chemical synthesis process of Pt nanoparticles. Asia Pac. J. Energy Environ. **1**(2), 107 (2014)
17. Mineo, H.; Masaru, H.: Preparation of dispersed Pt nanoparticles on a carbon nanostructured surface using supercritical fluid chemical deposition. Mater. J. **3**, 1559–1572 (2010). https://doi.org/10.3390/ma3031559

18. Calvillo, L.; Gangeri, M.; Perathoner, S.; Centi, G.; Moliner, R.; Lázaro, M.J.: Synthesis and performance of Pt supported on ordered mesoporous carbons as catalyst for PEM fuel cells: effect of the surface chemistry of the support. Int. J. Hydrogen Energy **36**, 9805–9814 (2011)
19. Bessel, C.A.; Kate, L.; Rodriguez, N.M.: Terry KBR (2001) Graphite nanofibers as an electrode for fuel cell applications. J. Phys. Chem. B. **105**(6), 1115–1118 (2001)
20. Antolini, E.: Formation, microstructural characteristics and stability of carbon supported platinum catalysts for low temperature fuel cells. J. Mater. Sci. **38**, 2995–3005 (2003)
21. Kvande, I.; Stein, T.B.; Mikhail, T.; Magnus, R.; Svein, S.; Reidar, T.; De, C.: On the preparation methods for carbon nanofiber-supported Pt catalysts. Topics Catal. **45**(1–4), 81–85 (2007). https://doi.org/10.1007/s11244-007-0244-5
22. Asanda, N.: Electrochemical investigation of Pt nanoparticles supported on carbon nanotubes as cathode electrocatalysts for direct methanol fuel cell. A thesis submitted in fulfillment of the requirements for the degree of Magister Scientiae in the Department of Chemistry, University of the Western cape 44–54 62 (2010)
23. Yehya, M.A.; Abdullah, A.; Ahmad, T.J.; Ma'an,, F.R.A.: Synthesis and characterization of carbon nanofibers grown on powdered activated carbon. J. Nanotechnol. **2016**, 1–10 (2016)
24. Idowu, A.O.: Development of a suitable bimetallic (Fe–Co) catalyst on kaolin support for carbon nanotube synthesis. ME Thesis Federal University of Technology, Minna (2016)
25. Mustafa, M.; Mohammed, A.; Rasel, D.: Optimization of the synthesis of superhydrophobic carbon nanomaterials by chemical vapor deposition. Sci. Rep. **8**, 1–12 (2018). https://doi.org/10.1038/s41598-018-21051-3
26. Chang-Seop, L.; Yura, H.: Preparation and Characterization of CNF and its Composites by Chemical Vapor Deposition, vol 1. Open Book Publication, pp 2–21 (2016)
27. Alhassan, M.I.: Formulation of bimetallic (Fe–Co) catalyst on $CaCO_3$ support for Carbon nanotube Synthesis. M.E. Thesis Federal University of Technology, Minna (2016)
28. Prabhu, T.G.: Green synthesis of noble metal of Pt Nanoparticles from *Ocimum sanctum* (Tulsi). IOSR J. Biotechnol. Biochem. (IOSR-JBB) **3**(1), 107–112 (2017). https://doi.org/10.9790/264x-0301107112
29. Viet-Long, N.; Nguyen, D.C.; Tomokatsu, H.; Hirohito, H.; Gandham, L.; Masayuki, N.: The synthesis and characterization of Pt nanoparticles: a method of controlling the size and morphology. J. Nanotechnol. **21**, 35–65 (2010). https://doi.org/10.1088/0957-4484/21/3/035605
30. Vinila, V.S.; Jacob, R.; Mony, A.; Nair, H.G.; Issac, S.; Rajan, S.; Nair, A.S.; Satheesh, D.J.; Isac, J.: X-ray diffraction analysis of nano crystalline ceramic $PbBaTiO_3$. Cryst. Struct. Theory Appl. **3**, 57–65 (2014)
31. Xubin, P.; Iliana, M.R.; Ray, M.; Jingbo, L.: Nanocharacterization and bactericidal performance of silver modified titania photocatalyst. Colloids Surf. B J. Biointerfaces **77**, 82–89 (2010)
32. Theivasanthi, T.; Alagar, M.: Nano sized copper particles by electrolytic synthesis and characterizations. Int. J. Phys. Sci. **6**(15), 3662–3671 (2011)
33. http://xpssimplified.com/elements/Pt.php
34. Jäger, R.; Härk, E.; Kasatkin, P.E.; Pikma, P.; Joost, U.; Paiste, P.; Aruväli, J.; Kallio, T.; Jiang, H.; Lust, E.: Carbide derived carbon supported Pt nanoparticles with optimum size and amount for efficient oxygen reduction reaction kinetics. J. Electrochem. Soc. **164**(4), 448–453 (2017)
35. Yu-chun, C.; Chia-chun, L.; Chun-ping, C.: Characterization of Pt nanoparticles deposited on functionalized graphene sheets. Mater. J. **8**, 6484–6497 (2015). https://doi.org/10.3390/ma8095318
36. Farokh, M.; Mohammad, J.; Soosan, R.Z.: Durability investigation and performance study of hydrothermal synthesized Pt-multi walled carbon nanotube nanocomposite catalyst for proton exchange membrane fuel cell. Energy J. (2017). https://doi.org/10.1016/j.energy.2017.07.098
37. Dongping, Z.; Jeyavelvel, M.; Michael, V.M.: Adsorption/desorption of hydrogen on Pt nanoelectrodes: evidence of surface diffusion and spillover. J. Am. Chem. Soc. (2009). https://doi.org/10.1021/ja902876v
38. Shukla, S.: Experimental analysis of inkjet printed polymer electrolyte fuel cell electrodes. PhD thesis, University of Alberta, Edmonton (2016)
39. Liang, H.; Koji, M.; Wenbin, G.; Chao-Yang, W.: Modeling and experimental validation of Pt loading and electrode composition effects in PEM fuel cells. J. Electrochem. Soc. **162**(8), 854–867 (2015)
40. Rashmi, S.; Singh, M.K.; Sushmita, B.; Ashish, S.; Kohli, D.K.; Prakash, C.G.; Meenakshi, S.; Gupta, P.K.: Facile synthesis of highly conducting and mesoporous carbon aerogel as Pt support for PEM fuel cells. Int. J. Hydrogen Energy (2017). https://doi.org/10.1016/j.ijhyd
41. Morawietz, T.; Handl, M.; Oldani, C.; Friedrich, K.A.; Hiesgen, R.: Influence of water and temperature on ionomer in catalytic layers and membranes of fuel cells and electrolyzers evaluated by AFM. In: 7th International Conference on Fundamentals and Development of Fuel Cell, pp 1–12 (2018). https://doi.org/10.1002/fuce.201700113
42. Young-Gab, C.; Chang-Soo, K.; Dong-Hyun, P.; Dong-Ryul, S.: Performance of a polymer electrolyte membrane fuel cell with thin film catalyst electrodes. J. Power Sources **71**, 174–178 (2012)
43. Neetu, J.; Palanisamy, R.; Elena, B.; Xiaojuan, T.; Feihu, W.; Mikhail, E.; Robert, C.H.: Functionalized single-walled carbon nanotube-based fuel cell benchmarked against US DOE 2017 technical targets. Sci. Rep. **3**, 2257 (2013)
44. Anwar, M.T.; Xiaohui, Y.; Shuiyun, S.; Naveed, H.; Fengjuan, Z.; Liuxuan, L.; Junliang, Z.: Enhanced durability of Pt electrocatalyst with tantalum doped titania as catalyst support. Int. J. Hydrogen Energy (2017). https://doi.org/10.1016/j.ijhyden
45. Jae-Young, L.; Jiyong, J.; Jae Kwang, L.; Sunghyun, U.; Eon-Soo, L.; Jae-Hyuk, J.; Nam-Ki, K.; Yong-Chul, L.; Jaeyoung, L.: Effect of hydrogen partial pressure on a polymer electrolyte fuel cell performance. Korean J. Chem. Eng. **27**(3), 843–847 (2010). https://doi.org/10.1007/s11814-010-0141-7
46. Shuang, M.A.; Mikkel, J.L.: Performance of the electrode based on silicon carbide supported Pt catalyst for proton exchange membrane fuel cells. J. Electroanal. Chem. **791**, 175–184 (2017)
47. Gazdzicki, P.; Mitzel, J.; Dreizler, A.M.; Schulze, M.; Friedrich, K.A.: Impact of Pt loading on performance and degradation of polymer electrolyte fuel cell electrodes studied in a rainbow stack. Fuel Cells **18**, 270–278 (2018). https://doi.org/10.1002/fuce.201700099